Synthesis, structure and magnetic properties of an inorganic–organic hybrid compound†

Sukhendu Mandal,[a] Mark A. Green,[b] Swapan K. Pati*[c] and Srinivasan Natarajan*[a]

Received 29th September 2006, Accepted 27th November 2006
First published as an Advance Article on the web 15th December 2006
DOI: 10.1039/b614186b

Hydrothermal reaction of a mixture of MnC_2O_4, H_3PO_3, piperazine and water at 423 K for 72 h resulted in a new inorganic–organic hybrid phase, $[C_4N_2H_{12}][Mn^{II}_2(HPO_3)_2(C_2O_4)]$, **I**. The structure comprises a network of Mn_2O_{10} dimers, HPO_3 psuedo-tetrahedra and oxalate units, connected through their vertices forming a three-dimensional structure with one-dimensional channels. Protonated piperazine molecules are found in the channels. The formation of $Mn(HPO_3)_\infty$ layers using only one type of secondary building unit, SBU-4, is noteworthy. Detailed magnetic investigations reveal that the antiferromagnetic layers are coupled in such a way to show magnetic polarizations on application of high magnetic field at low temperatures. This is unique and to the best of our knowledge has been observed for the first time in an open-framework solid.

Introduction

Research in the area of open-framework materials continues to be of interest not only because of the wide diversity in structures, but also for their many applications in the areas of catalysis, sorption and separation processes.[1] Of the various inorganic open-framework materials discovered during the last decade or so, the metal phosphates are an important class. The family of open-framework metal phosphates includes zero-dimensional molecular structures, one-dimensional chains or ladders, two-dimensional layers and three-dimensional structures.[2] The introduction of rigid organic linkers, such as oxalates, as part of the inorganic framework has opened up tremendous possibilities for research in this area giving rise to new inorganic–organic hybrid compounds.[3,4] In most of these compounds, the important structural feature appears to be the presence of metal phosphate chains/ladders or sheets, cross-linked by the oxalate units giving rise to the three-dimensional structure. Recently, it has been shown that the traditional phosphate tetrahedra can be replaced by the pseudo-tetrahedral hydrogenphosphite, $[HPO_3]^{2-}$, oxoanion with some success.[5,6] While many phosphate–oxalate hybrid networks have been prepared and characterized,[3,4] the exploratory research on phosphite–oxalate frameworks have only just begun.[7–9]

Most of the syntheses of open-framework compounds have been carried out under hydrothermal conditions, which involve multi-component heterogeneous reactions and complex processes, such as equilibrium reactions, nucleation and growth and so on, occurring simultaneously.[10] The rational design and synthesis of open-framework compounds are far from reality due to the interplay of many factors such as oxidation states and coordination preferences of the metal ions, stereochemistry of the ligand, solvent effects, the nature of the counter ion, *etc*. Though the synthesis process is far from understood, the tetrahedral open-framework zeolitic and related structures have been described and rationalized by the identification of simpler units, known as secondary building units (SBUs).[11] The SBU approach has also been quite successful in the description of many framework structures based on octahedral–tetrahedral units[12] and also for the recently discovered inorganic–organic hybrids.[13]

Compounds possessing octahedral–tetrahedral networks are generally transition metal phosphates and related systems exhibiting a variety of open-framework structures. Transition metal compounds, in general, exhibit interesting properties due to the presence of uncompensated spins. Some of the compounds undergo large quantum fluctuations, at low temperatures, giving rise to interesting magnetic phenomena, such as finite spin gap, short range magnetic order, *etc*.[14,15] The observation of spin-Peierls transition in $CuGeO_3$,[16,17] and gapped and gapless behavior in the series of compounds of the general formula $Sr_{n-1}Cu_{n+1}O_{2n}$ (n = 3,5,7,…),[14,18,19] *etc.* has generated considerable interest in this area of research. Furthermore, the magnetic interactions in the low-dimensional structures can be coupled *via* suitable linkers giving rise to interesting magnetic properties.[20] In this connection, the transition metal based inorganic–organic hybrid solids provide ideal systems to investigate such effects.

We have been investigating phosphite–oxalate hybrid compounds not only with a view to producing new materials but also to unravel the subtle structural features that characterize these solids.[7–9] During the course of these investigations, we have now isolated a manganese phosphite–oxalate of the

[a]*Framework Solids Laboratory, Solid State and Structural Chemistry Unit, Indian Institute of Science, Bangalore 560 012, India. E-mail: snatarajan@sscu.iisc.ernet.in*
[b]*The Davy-Faraday Research Laboratory, The Royal Institution of Great Britain, 21 Albemarle Street, London, UK W1S 4BS*
[c]*Theoretical Sciences Unit, Jawaharlal Nehru Centre for Advanced Scientific Research, Jakkur P.O., Bangalore 560 064, India. E-mail: pati@jncasr.ac.in*

† Electronic supplementary information (ESI) available: TGA, IR and UV-Vis spectra, and asymmetric unit of **I**; plot of thermal variation of dc susceptibility. See DOI: 10.1039/b614186b

formula $[C_4N_2H_{12}][Mn^{II}_2(HPO_3)_2(C_2O_4)]$, **I**. The structure of **I** consists of edge shared Mn_2O_{10} dimers linked by the HPO_3 units forming infinite two-dimensional neutral inorganic layers, $[Mn(HPO_3]_\infty$, which are pillared on either side by the oxalate anions giving rise to the three-dimensional structure with channels. Interesting magnetic properties have been observed on application of a magnetic field to this compound. In this article, we present the synthesis, structure and magnetic studies of **I**.

Experimental

Synthesis and initial characterization

The manganese phosphite–oxalate $[C_4N_2H_{12}][Mn^{II}_2(HPO_3)_2(C_2O_4)]$, **I**, was synthesized under hydrothermal conditions using manganese oxalate as the source of manganese. In a typical synthesis, 0.277 g of manganese oxalate was dissolved in 7 mL of deionized water. To this, 0.318 g of H_3PO_3 was added. Finally, 0.334 g of piperazine (PIP) was added to the mixture and homogenized for 30 min at room temperature. The final mixture with the composition 2.0 MnC_2O_4 : 4.0 H_3PO_3 : 4.0 PIP : 400 H_2O was transferred into a 23 mL PTFE-lined acid-digestion bomb and heated at 150 °C for 72 h. The resulting product contained only light pink cube-like single crystals in large quantities. The crystals were filtered, washed with deionized water, and dried at ambient conditions. The yield of the product was ~75% based on Mn. The initial pH of the reaction mixture was ~4 and the pH value did not show any appreciable change during the hydrothermal reaction.

The initial characterization was carried out using powder X-ray diffraction (XRD), thermogravimetric analysis (TGA) and infrared (IR) spectroscopy measurements. EDAX analysis indicated a Mn : P ratio of 1 : 1, which is in agreement with the molecular formula obtained from the single crystal structure. Elemental analysis: obsd (calcd): C 16.70 (16.15), H 3.41 (3.16), N 5.28 (6.28%). The powder XRD patterns were recorded on crushed single crystals in the 2θ range 5–50° using Cu Kα radiation (Philips X'pert, Pro). The XRD pattern was entirely consistent with the pattern simulated from the structure determined using the single-crystal X-ray diffraction (Fig. 1).

Thermogravimetric analysis (TGA) was carried out (Mettler-Toledo, TG850) in air (flow rate = 50 mL min^{-1}) in the temperature range 25–800 °C (heating rate = 5 °C min^{-1}). The results show a single sharp weight loss in the range 350–450 °C. The total weight loss was found to be 35.65%, which corresponds with the loss of the organic amine and the decomposition of the oxalate unit along with the oxidation of P^{III} to P^{V}. The final decomposed product was found to be crystalline and the powder XRD pattern corresponds to $Mn_2P_2O_7$ (JCPDS: 35-1497).

Infrared (IR) spectroscopy studies were carried out in the range 400–4000 cm^{-1} using the KBr pellet method (Perkin Elmer, spectrum 1000). The IR spectrum of **I** shows the characteristic bands for the protonated piperazine molecule, HPO_3 unit and the oxalate moiety. The observed IR bands are: ν(NH) 3224 cm^{-1}, ν(CH) = 2985 cm^{-1}, ν(PH) = 2362 cm^{-1}, ν_{as}(CO) = 1626 cm^{-1}, δ(CH) = 1470 cm^{-1}, ν_s(CO) = 1365 cm^{-1}, $\nu_{as}(PO_3)$ = 1117 cm^{-1}, δ(HP) = 1071 cm^{-1}, $\nu_s(PO_3)$ = 1046 cm^{-1}, $\delta_s(PO_3)$ = 573 cm^{-1}, $\delta_{as}(PO_3)$ = 486 cm^{-1}.

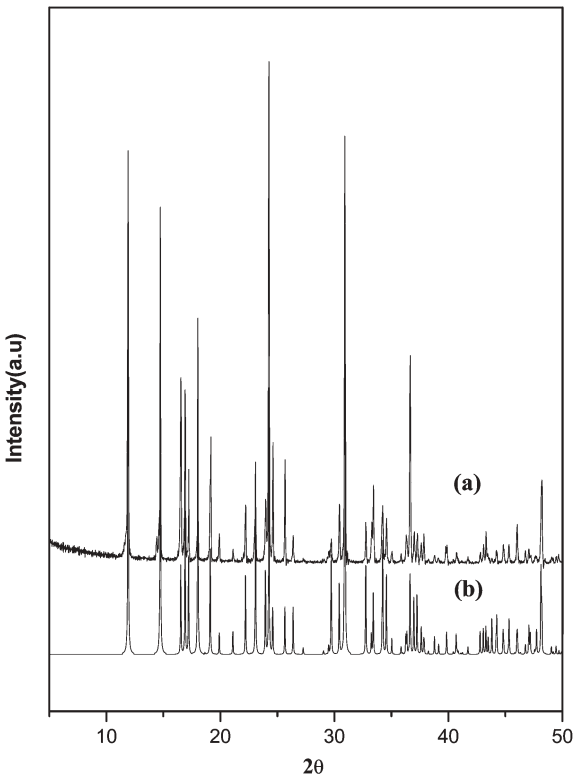

Fig. 1 Powder X-ray diffraction patterns (Cu Kα) of $[C_4N_2H_{12}][Mn^{II}_2(HPO_3)_2(C_2O_4)]$, **I**: (a) experimental, (b) simulated.

Single crystal structure determination

The single crystal data were collected on a Bruker AXS smart Apex CCD diffractometer at 293(2) K, using Mo Kα (λ = 0.71073 Å) radiation. Data were collected with a ω scan width of 0.3°. A total of 606 frames were collected in three different setting of φ (0, 90, 180°) keeping the sample-to-detector distance fixed at 6.03 cm and the detector position (2θ) fixed at −25°. The structure was solved and refined using SHELXL-97 present in the WinGx suit of programs (Version 1.63.04a).[21] All the hydrogen positions were initially located in the difference Fourier maps, and for the final refinement, the hydrogen atoms were placed in geometrically ideal positions and refined in the riding mode. Final refinement included atomic positions for all the atoms, anisotropic thermal parameters for all the non-hydrogen atoms, and isotropic thermal parameters for all the hydrogen atoms. Full-matrix least-squares refinement against $|F|^2$ was carried out using the WinGx package of programs.[21] Details of the structure solution and final refinements for **1** are given in Table 1. CCDC reference number 272629. For crystallographic data in CIF or other electronic format see DOI: 10.1039/b614186b

Results and discussion

The asymmetric unit contains one crystallographically distinct Mn and one crystallographically distinct P atom. The Mn is octahedrally coordinated by six oxygen atoms with Mn–O

Table 1 Crystal data and structure refinement parameters for $[C_4N_2H_{12}][Mn_2^{II}(HPO_3)_2(C_2O_4)]$, **I**[a]

Empirical formula	$C_6H_{14}N_2O_{10}P_2Mn_2$
Formula weight	445.988
Crystal system	Monoclinic
Space group	$P2_1/c$ (no. 14)
a/Å	6.0627(8)
b/Å	10.7122(15)
c/Å	10.3872(14)
β/deg	97.956(3)
Volume/Å^3	668.10(2)
Z	2
T/K	293(2)
ρ_{calc}/g cm^{-3}	2.217
μ/mm^{-1}	2.186
θ range/deg	2.75 to 27.96°
F(000)	448
λ(Mo Kα)/Å	0.71073
Reflection collected	5613
Unique reflections	1569
Number of parameters	100
Goodness of fit	1.146
R indexes [$I > 2\sigma(I)$]	$R_1 = 0.0353$, $wR_2 = 0.1035$
R (all data)	$R_1 = 0.0364$, $wR_2 = 0.1041$
Largest diff. peak and hole/e Å^{-3}	0.953 and −0.954

[a] $R_1 = \Sigma||F_o| - |F_c||/\Sigma|F_o|$; $wR_2 = \{\Sigma[w(F_o^2 - F_c^2)]/\Sigma[w(F_o^2)^2]\}^{1/2}$. $w = 1/[\rho^2(F_o)^2 + (aP)^2 + bP]$. $P = [\max(F_o,O) + 2(F_c)^2]/3$, where $a = 0.0551$ and $b = 1.4949$.

bond distances in the range 2.074(2)–2.315(2) Å and O–Mn–O bond angles in the range of 72.26(8)–163.27(8)°. The Mn atoms are connected to both the phosphite and oxalate moieties through the oxygens. The P atom has three P–O–Mn bonds and one P–H bond. The P–O bond distances have an average value of 1.522 Å and average O–P–O bond angle of 112.41°. Selected bond distances are given in Table 2.

The framework structure of **I** comprises a network of MnO_6 octahedra, HPO_3 pseudo-tetrahedra and C_2O_4 units linked through their vertices. The MnO_6 octahedra share two oxygen atoms and are connected through their edges forming Mn_2O_{10} dimers, which are capped on either side by HPO_3 units forming the basic secondary building unit. This building unit resembles one of the secondary building units, SBU-4, proposed by Ferey[12] to explain complex open-framework structures formed by the gallium and iron phosphates. The SBU-4 units in **I** are connected through the corners *via* the oxygens giving rise to two-dimensional layers of the formula $[Mn^{II}(HPO_3)]_\infty$, which are neutral (Fig. 2a). The oxalate units anchor on to this layer on either side, acting as a pillar forming the anionic inorganic–organic hybrid structure with one-dimensional channels (Fig. 2b). Charge compensation is achieved by the presence of protonated piperazine cations, which occupy the middle of the channels (Fig. 2b). The close proximity between the piperazine molecules and the framework also gives rise to hydrogen bond interactions. The following hydrogen bonds have been observed: C(2)–H(2A)···O(3) (H–A = 1.81 Å, D–H···A = 169°) and C(2)–H(2B)···O(1) (H–A = 1.92 Å, D–H···A = 150°).

Table 2 Selected bond distances and angles in $[C_4N_2H_{12}][Mn_2^{II}(HPO_3)_2(C_2O_4)]$, **I**[a]

Bond	Distance/Å	Bond	Distance/Å
Mn(1)–O(1)#1	2.074(2)	Mn(1)–O(4)#2	2.315(2)
Mn(1)–O(2)#2	2.149(2)	P(1)–O(1)	1.528(2)
Mn(1)–O(3)	2.156(2)	P(1)–O(2)	1.506(2)
Mn(1)–O(4)	2.205(2)	P(1)–O(3)	1.533(2)
Mn(1)–O(5)#3	2.214(2)		

[a] Symmetry transformations used to generate equivalent atoms: #1 $-x, y - 1/2, -z + 3/2$; #2 $-x, -y + 1, -z + 1$; #3 $x + 1, y, z$.

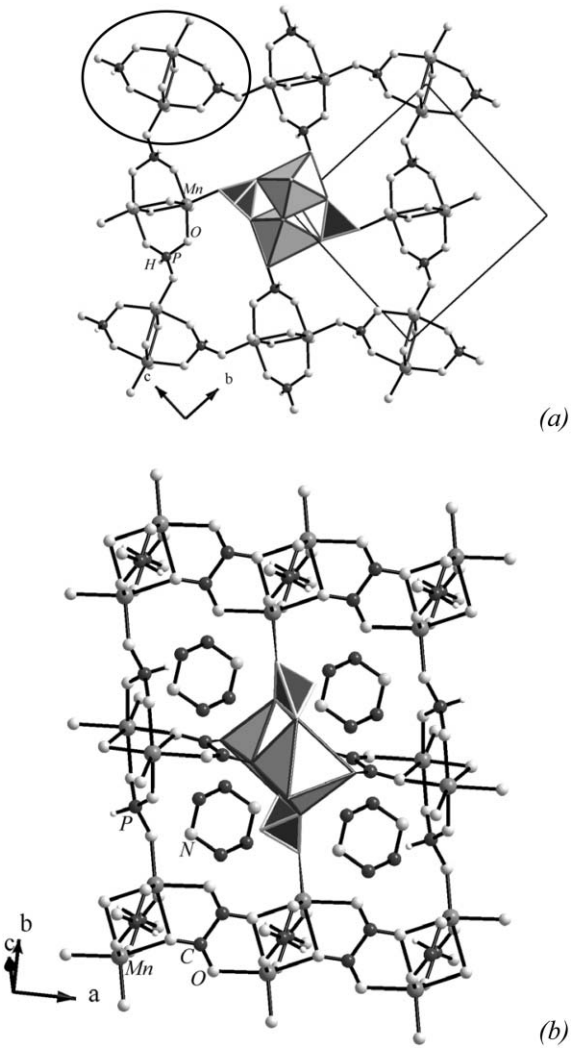

Fig. 2 (*a*) View of the inorganic layer in $[C_4N_2H_{12}][Mn^{II}_2(HPO_3)_2(C_2O_4)]$, **I**, showing the connectivity between the SBU-4 units (see text). The circle shows the SBU-4 unit. (*b*) The structure of **I** in the *ab* plane. Note that the inorganic layers are cross-linked by the oxalate units.

It is to be noted that the inorganic part of the hybrid structure of **I** has been realized in an iron arsenate, $[C_{10}N_4H_{28}][\{FeF(OH)(HAsO_4)\}_4]$,[22] and in a vanadium arsenate, $Ba_2VO_2(AsO_4)$.[23] Both the compounds have anionic layered framework structures, and are built up exclusively by the corner sharing of SBU-4 units. Charge compensation is achieved by the presence of protonated triethylenetetramine molecules in the structure of the iron arsenate and by barium cations in the vanadium arsenate. The inorganic part (manganese phosphite, $[Mn^{II}(HPO_3)]_\infty$) in **I**, on the other hand, is neutral. This is the first observation of SBU-4 units,[12] to our knowledge, in phosphite–oxalate structures.

It is worthwhile to compare the structure of **I** with other similar hybrid structures formed using the same organic amine, piperazine (Fig. 3). The synthesis, structure and properties of few phosphite–oxalates have been reported earlier by us.[7–9] Thus, iron and cobalt phosphite–oxalate compounds with the formula $[(C_4N_2H_{12})M_4(HPO_3)_2(C_2O_4)_3]$ (M = Fe, Co) have been prepared using piperazine. In both these compounds, the edge-shared MO_6 octahedra form $[M_2O_{10}]$ dimers, similar to **I**. But the connectivity involving the dimers, phosphite and oxalate units creates distinct differences between the three-dimensional framework structures of Fe and Co when compared to Mn. In the $[(C_4N_2H_{12})M_4(HPO_3)_2(C_2O_4)_3]$ (M = Fe, Co) structures, the $[M_2O_{10}]$ dimers were connected together through their corners forming infinite one-dimensional M–O–M chains. The HPO_3 groups were grafted onto these chains and appear not to contribute to the extended connectivity of the structure. The framework structure was, in fact, built up exclusively by the connectivity between the infinite one-dimensional M–O–M chains and the oxalate units. The phosphite units essentially satisfy the coordination requirements of the central transition element (Fig. 3a). This situation needs to be contrasted with the structure of **I**. In **I**, the phosphite units links the Mn_2O_{10} dimers in such a way that they form SBU-4 units,[12] which are bonded through the corners giving rise to a two-dimensional inorganic layer $[Mn^{II}(HPO_3)]_\infty$. The oxalate units connect the layers to give the three-dimensional structure (Fig. 3b).

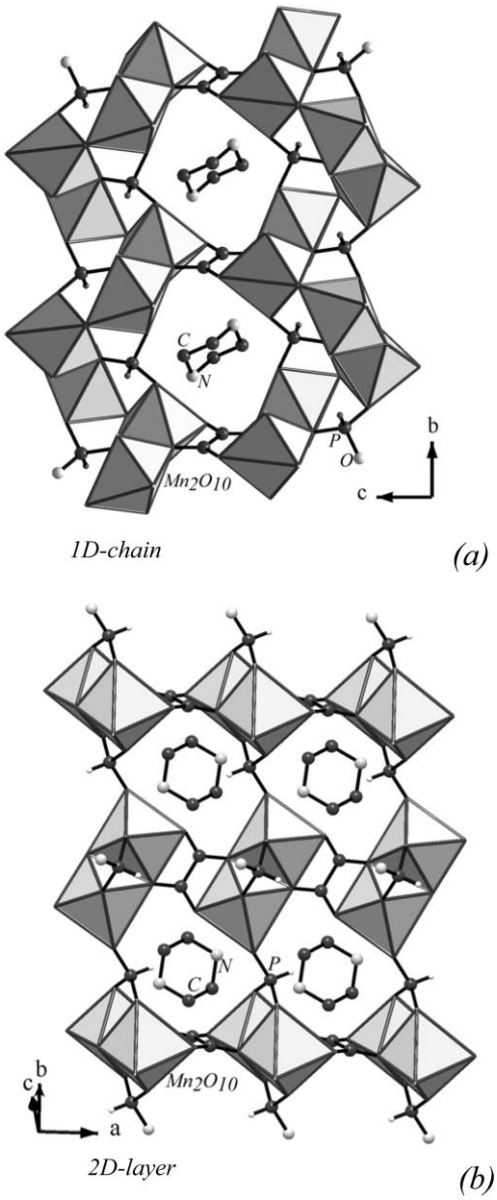

Fig. 3 (*a*) Structure of $[(C_4N_2H_{12})M_4(HPO_3)_2(C_2O_4)_3]$ (M = Fe, Co) showing the connectivity between the M–O–M chains and oxalate units. (*b*) Structure of **I** showing the connectivity between the two-dimensional $[Mn(C_2O_4)]_\infty$ layers and oxalate units. Note the subtle differences in the connectivity between the M_2O_{10} dimers and HPO_3 units (see text).

The presence of Mn^{II} dimers, coupled through the phosphite and oxalate units, indicated the possibility of interesting magnetic properties in **I**. Magnetic susceptibility studies have been performed on powdered single crystals in the temperature range 300–2 K using a SQUID magnetometer. Fig. 4 shows the temperature dependence of the magnetic susceptibility in both field-cooled (FC) and zero field-cooled (ZFC) conditions. In the insets, reciprocal susceptibilities and the effective magnetic moment are plotted. At high temperatures ($T > 100$ K) the thermal evolution of χ_M follows a Curie–Weiss law, $\chi = C/(T - \theta)$, with $\theta = -24.55$ K and $C = 0.1968$ cm^{-3} K. The ZFC and FC dc susceptibilities exhibit marked differences as the temperature is lowered below $T = 7$ K.

The observed maximum in magnetic susceptibility at low temperature ($\sim$16 K) is in general associated with short-range magnetic order in low-dimensional antiferromagnetic systems.[24] Since the spin magnitude of Mn^{2+} is 5/2, the classical spin concept can be used with the well known Fisher formula.[25] The temperature dependence of the ZFC data can be fitted with an inverse temperature form for χ, equivalent to an expression obtained for the dimer, $\chi = A\exp(-\Delta/K_BT)/(K_BT)^\tau$, where Δ is the spin gap and τ is an exponent relating the extended nature of the antiferromagnetic interactions

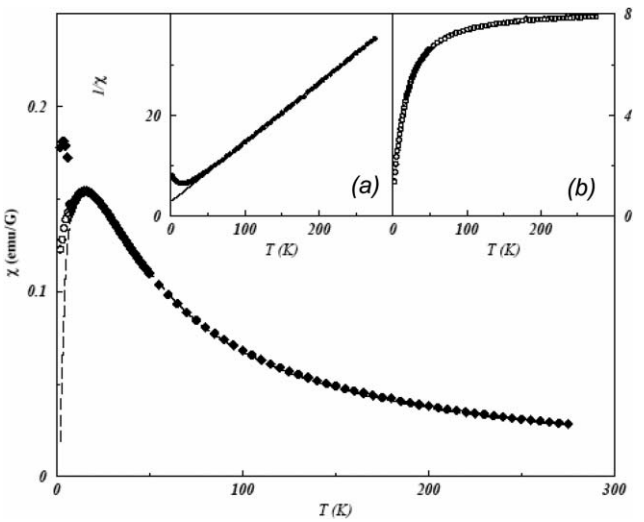

Fig. 4 Thermal variation of ZFC (open circles) and FC (filled circles) dc susceptibility. Note the difference between the two (see text). Insets show the variation of (a) $1/\chi$ and (b) μ_{eff} as a function of temperature.

within the system. For a simple dimer, $\tau = 1$ and it takes a value close to 0.5 for a truly extended lattice system. By fitting the above form of the susceptibility, χ, with the experimental data, we find that the best fit is obtained with $\Delta = 13.5$ K and $\tau = 0.55$ (dashed line in Fig. 4). Clearly this exponent gives an idea of the optimum length scale for the exchange processes at a temperature corresponding to the maximum of χ. Note that the FC data follow the ZFC data even below the maximum.

To understand whether the ZFC/FC data divergence is associated with some randomness or spin-glass transition as is found in many materials,[26] we carried out ac susceptibility studies. In the ac measurement, the magnetization of the sample responds to the oscillating external magnetic field and is very sensitive to the slope of $M(H)$ so that small magnetic shifts can be detected even when the absolute magnetic moment is large. Both the in-phase and out-of-phase shift susceptibility components (χ' and χ'') are plotted in Fig. 5 for a number of ac frequencies. It may be noted that while the χ'' data remain unchanged with T, the χ' data exhibit a cusp at around $T = 7$ K. The cusp in χ' corresponds to the freezing temperature of the magnetization data.[27] However, in our case, the location of the cusp remains unchanged for all the measured frequencies, a feature that is clearly distinct from spin-glass behavior. Moreover, the cusp behavior of χ' is at the same temperature where the dc ZFC/FC data diverge (see Fig. 4). Interestingly, such behavior is completely absent in χ'', indicating that at low temperature the magnetic phenomenon is driven by dissipative processes.

Since the χ' (slope of $M(H)$ curve) values show a cusp, to understand the nature of the exchange processes as a function of magnetic field, we studied the dc magnetization phenomena in detail. Even at low temperature, the magnetization does not show hysteresis behavior, as expected. However, the effect of the magnetic field in controlling the magnetization behavior, particularly at high field strength, turned out to be quite interesting. For a complete understanding, both the FC and ZFC dc magnetization data are shown in Fig. 6 for a range of field strengths. While the field-cooled measurements are

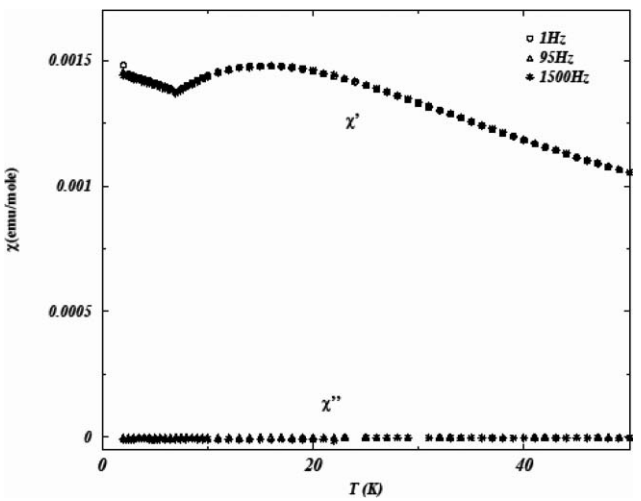

Fig. 5 The thermal variation of the ac susceptibility at different frequencies. Note the marked differences in the in-plane (χ') and the out-of-plane (χ'') magnetic susceptibilities.

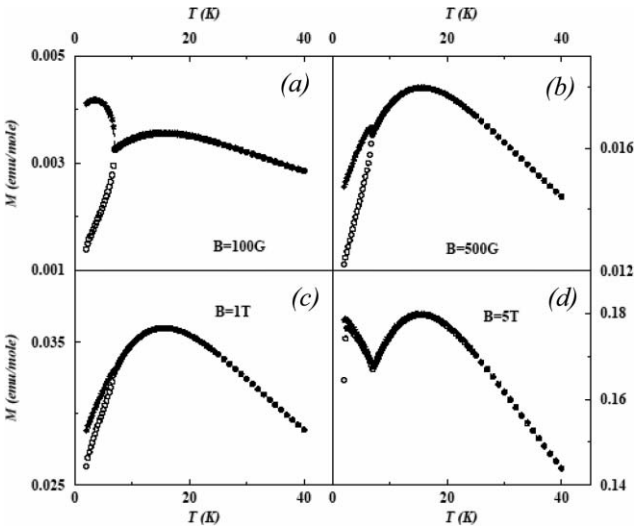

Fig. 6 The thermal variation of dc susceptibility as a function of different applied fields (ZFC (open circles) and FC (filled circles); see text).

expected to show alignment of the spins at low temperature, the extent of which will depend on the strength of the field, the zero-field cooled measurements are expected to be devoid of any alignment of the magnetic spins. Below the T_{cusp}, the magnetization appears to be very small, especially for field strengths above 100 G (Fig. 6). For weak fields, the ZFC data suggest ordering at low temperatures and the FC data show an upward rise after T_{cusp}, as expected.

The magnetization studies at larger field strengths, on the other hand, appear to be quite different. Near the transition temperature (T_{cusp}), both the FC and ZFC data start decreasing with different slopes (Fig. 6b and c).[28] Neither the ZFC nor the FC data approach zero as T is reduced further from T_{cusp} for $H = 5$ T (Fig. 6d), instead both ZFC and FC data start increasing at $T \sim 2$ K $< T_{cusp}$. This, probably, corresponds to a very weak magnetic polarization and occurs only at very low temperature (at $T = 2$ K for $H = 5$ T and $T = 7$ K for $H = 10$ T (see ESI†).

The above observations may be rationalized by examining the crystal structure of **I**. The two-dimensional planes are comprised of the Mn^{2+} dimers (M–M distance = 3.265 Å) and HPO_3 ligands (dimer–phosphate distance = 5.9071 Å). The out of plane connectivity is through the oxalate (dimer–oxalate distance = 6.068 Å), which is weak and does not contribute down to T_{cusp}. However, this picture appears to be valid only for small magnetic fields. At strong fields and at temperatures below T_{cusp}, however, the moments in the manganese phosphite plane start interacting with the moments in the neighboring plane through the oxalate units. The dramatic rise in the magnetization with $H = 5$ and 10 T (see ESI†) suggests that below $T = 2$ K and 7 K, respectively, the system goes through a transition point whereby the geometry induced exchanges become important. This is possibly due to the combined effect of Dzyaloshinskii–Moriya and field dependent chiral moments.[29,30] Because of its weak strength, this interaction becomes relevant only at very small K_BT and for high H values.

Conclusions

The synthesis, structure and properties of a new inorganic–organic hybrid compound, $[C_4N_2H_{12}][Mn^{II}_2(HPO_3)_2(C_2O_4)]$, **I**, has been accomplished. The structure consists of Mn_2O_{10} dimers connected by HPO_3 forming SBU-4 units, which are connected to give rise to $Mn(HPO_3)_\infty$ inorganic layers. The layers are cross-linked by oxalates forming the three-dimensional structure. The formation of layers with only one type of SBU-4 unit is noteworthy. Magnetic studies reveal that the anti-ferromagnetic interactions between Mn^{II} spins within the two dimensions prevail over a range of temperature. The observation of field dependent geometry induced exchange components at low temperatures is important. The present structure along with the earlier reported phosphite–oxalate structures clearly indicate that this family of compounds is also likely to exhibit the wide structural and compositional diversity observed in the phosphate–oxalate hybrid structures. The novel magnetic properties observed in **I** also prompt us to believe that it is worthwhile to explore the synthesis of other phosphite–oxalate compounds. Work on this theme is currently in progress.

Acknowledgements

SN and SKP thank the Department of Science and Technology (DST), Government of India, for the award of research grants. The authors also thank DST-IRPHA for the CCD facility.

References

1 A. K. Cheetham, T. Loiseau and G. Ferey, *Angew. Chem., Int. Ed.*, 1999, **38**, 3268 and references therein.
2 C. N. R. Rao, S. Natarajan, S. Neeraj, A. Choudhury and A. A. Ayi, *Acc. Chem. Res.*, 2001, **34**, 80.
3 M. F. Tang and K. H. Lii, *J. Solid State Chem.*, 2004, **177**, 1912.
4 A. Choudhury, S. Natarajan and C. N. R. Rao, *Chem.–Eur. J.*, 2000, **6**, 1168.
5 W. T. A. Harrison, M. L. F. Philips, J. Stranchfield and T. M. Nenoff, *Inorg. Chem.*, 2001, **40**, 895.
6 S. Fernandez, J. L. Mesa, J. L. Pizarro, L. Lezama, M. I. Arriortua and T. Rojo, *Angew. Chem., Int. Ed.*, 2002, **41**, 3683.
7 S. Mandal, S. K. Pati, M. A. Green and S. Natarajan, *Chem. Mater.*, 2005, **17**, 2912.
8 S. Mandal, M. A. Green and S. Natarajan, *J. Solid State Chem.*, 2005, **178**, 2376.
9 S. Mandal and S. Natarajan, *Chem.–Eur. J.*, 2006, DOI: 10. 1002/chem.200601026.
10 M. E. Davis and R. F. Lobo, *Chem. Mater.*, 1992, **4**, 756; G. Ferey, *C. R. Acad. Sci., Ser. II*, 1998, 1.
11 *Atlas of zeolite framework types*, ed Ch. Baerlocher, W. M. Meier and D. H. Olson, Elsevier, Amsterdam, 2001.
12 G. Ferey, *Chem. Mater.*, 2001, **13**, 3084; G. Ferey, *J. Solid State Chem.*, 2000, **152**, 37 and related articles in the same issue; G. Ferey, *J. Fluorine Chem.*, 1995, **72**, 187.
13 N. W. Ockwig, O. Delgado-Friedrichs, M. O'Keeffe and O. M. Yaghi, *Acc. Chem. Res.*, 2005, **38**, 176 and related articles in the same issue.
14 F. D. M. Haldane, *Phys. Lett.*, 1983, **93A**, 464; *Phys. Rev. Lett.*, 1983, **50**, 1153.
15 H. Hase, I. Terasaki and K. Uchinokura, *Phys. Rev. Lett.*, 1993, **70**, 3651.
16 M. Nishi, O. Fujita and J. Akimitsu, *Phys. Rev. B*, 1994, **50**, 6508.
17 E. Dagotto and T. M. Rice, *Science*, 1996, **271**, 618.
18 Z. Hiroi, M. Azuma, M. Takano and Y. Bando, *J. Solid State Chem.*, 1991, **95**, 230; M. Azuma, Z. Hiroi, M. Takano, Y. Bando and Y. Takeda, *Nature*, 1992, **356**, 775.
19 M. Azuma, Z. Hiroi, M. Takano, K. Ishida and Y. Kataoka, *Phys. Rev. Lett.*, 1994, **73**, 3463.
20 S. Mandal, S. K. Pati, M. A. Green and S. Natarajan, *Chem. Mater.*, 2005, **17**, 638.
21 G. M. Sheldrick, *SHELXL-97, Program for Crystal Structure Solution and Refinement*, University of Göttingen, Germany, 1997; L. J. Farrugia, *J. Appl. Crystallogr.*, 1999, **32**, 837.
22 S. Chakrabarty, S. K. Pati, M. A. Green and S. Natarajan, *Eur. J. Inorg. Chem.*, 2003, 3820.
23 F. Gagnard, C. Reisner and W. Tremel, *Inorg. Chem.*, 1997, **36**, 352.
24 R. Chitra, S. K. Pati, H. R. Krishnamurthy, D. Sen and S. Ramasesha, *Phys. Rev. B*, 1995, **52**, 6581.
25 M. E. Fisher, *Am. J. Phys.*, 1964, **32**, 343.
26 T. Johnson, K. Jonason, P. Jonsson and P. Nordblad, *Phys. Rev. B*, 1999, **59**, 8770.
27 J. A. Mydosh, *J. Magn. Magn. Mater.*, 1996, **157/158**, 606.
28 Note that at 500 G, the FC component shows both a hump (like 100 G data) and a decrease (like $B > 500$ G data) reminiscent of a weak field component near T_{cusp}.
29 T. Moriya, *Phys. Rev.*, 1960, **120**, 91.
30 D. Parihari and S. K. Pati, *Phys. Rev. B*, 2004, **70**, 180403R.